

# Impact of thermosiphoning on long-term behavior of closed-loop deep geothermal systems for sustainable energy exploitation



Morteza Esmailpour <sup>a,\*</sup>, Maziar Gholami Korzani <sup>b</sup>, Thomas Kohl <sup>a</sup>

<sup>a</sup> Institute of Applied Geosciences, Karlsruhe Institute of Technology, Karlsruhe, Germany

<sup>b</sup> School of Civil & Environmental Engineering, Queensland University of Technology, Queensland, Australia

## ARTICLE INFO

### Article history:

Received 13 February 2022

Received in revised form

25 May 2022

Accepted 4 June 2022

Available online 9 June 2022

### Keywords:

Closed geothermal system  
Deep geothermal exploitation  
Sustainable power generation  
Natural convection  
Thermosiphon effect

## ABSTRACT

Circulation of working fluid in closed geothermal loops is an alternative environmentally friendly approach to harvest subsurface energy compared to open hole geothermal doublet systems. However, the rapid decline of production temperature, low generated thermal power, and difficulties in deepening the system are major limitations. Herein, synthetic studies are presented to investigate the system's performance and improve its longevity for better use of this clean baseload power. The investigations are conducted by implementing appropriate equations of state to model state-of-the-art thermal and hydraulics processes in wellbores and considering various geometrical configurations to adopt proper design strategies. They provide insight for maximizing the generated thermal power, decreasing pumping energy, and avoiding production temperature drawdown. The results indicate that a stable thermal condition could be reached in which not only the temperature breakthrough is avoidable, but also the generated thermal power and production temperature continuously enhance over the project lifetime of one century. Analysis of the thermosiphon effect in the designed systems revealed that even with the pressure loss of 900 kPa at surface installations, the triggered natural flow rate is larger than 11 L/s. This thermosiphon flow rate yields the thermal power production of 2 MW and Cumulative extracted energy of 15 PJ over the project lifetime of 100 years. Restriction of this flow rate to 5 L/s leads to an average extraction temperature of 80 °C. It is also found that a change in the subsurface temperature gradient does not affect the optimal 2 km isolation length of the production well.

© 2022 The Authors. Published by Elsevier Ltd. This is an open access article under the CC BY license (<http://creativecommons.org/licenses/by/4.0/>).

## 1. Introduction

The possibility to continually extract heat from different geological systems (e.g., hydrothermal [1,2], geo-pressurized [3], EGS systems [4], hot dry rock [5], and magma [6]) makes geothermal energy an exciting option responding to the increase of global energy demand and mitigating harmful environmental impacts of fossil fuels [7]. However, seismic events induced by hydraulic fracturing and excess pressure, subsurface water contamination, uncertainties in geothermal field characterization [8], and the considerable drilling costs are significant barriers to the spread of open geothermal systems [9–11]. Borehole heat exchangers (BHEs) equipped with heat pumps can sustainably harvest geothermal energy without the aforementioned hazards [12–19]. Despite the power consumption of the heat pump, they

are economically beneficial and are successfully implemented by large numbers for single dwellings [20]. Their worldwide installed capacity has increased from 1.8 GW in 1995 to 50 GW in 2015 [21], and the total number of installed systems in Europe exceeds 1.9 million units [22]. The typical thermal power generation of BHE systems is approximately 50 W/m [23]. Moreover, retrofitting abandoned wells [24–26], as so-called “Deep BHE” [27,28], have recently received particular attention. The existence of 20–30 million abandoned wells [25] promotes the global tendency to retrofit them as geothermal systems and to produce a considerable amount of cost-effective energy by cutting the drilling cost.

Several studies have been conducted to improve the performance of BHEs by extending the heat exchange surface. Based on these studies, the BHEs can be categorized into four main groups: coaxial BHE [29], single U-tube BHE [30], double U-tube BHE [31], and helical BHE [32–34]. The double U-tube BHE comprises two connected U-tubes inside one borehole requires rather large well-bore diameters. Similarly, the coaxial BHE consists of a small “upflow” production pipe wrapped in a larger “downflow” injection

\* Corresponding author.

E-mail address: [morteza.esmailpour@kit.edu](mailto:morteza.esmailpour@kit.edu) (M. Esmailpour).

pipe, forming an annular cross-section, which requires a relatively large wellbore diameter to maintain suitable fluid velocities in the inner and outer pipes. Although the heat exchange area of helical BHE is more extensive than the other BHEs, helical pipe, which is made of special flexible materials, should be installed on a reinforced frame to strengthen its structure. In conclusion, the helical BHE system also suffers from large overall diameter which restricts its application in geothermal energy utilization. Furthermore, the economic viability of this system at high temperatures is a controversial issue since this thermal condition can deform its structure, which is commonly made of polyethylene (PE) and polyvinyl chloride (PVC) [35]. Nowadays, double U-tube and helical BHEs are installed as prefabricated structures with large overall diameters, which can be an obstacle to deepening these systems.

Recent development in drilling technologies [36–39] made drilling of deep inclined boreholes (i.e., the dip angle of greater than 90 deg. at several km depths) with complex trajectories feasible [40]. It allows for employing a rather new closed-loop deep geothermal (CDG) systems with a lengthy horizontal extension to exploit geothermal energy from both hydrothermal systems and hot dry rock. This CDG system consists of two vertical wellbores connected through an extended long horizontal well. Based on the geometrical configuration of this system, it is expected to obtain higher production temperature and thermal power compared to the conventional BHEs due to its operating depth and extended heat exchange surface area. To the best of our knowledge, the performance of a similar system possessing relatively shorter vertical and horizontal wellbores is experimentally evaluated in the north of Canada [41], and few studies have investigated its heat extraction mechanism numerically.

After having conducted a systematic literature review on the design and heat transfer of deep closed systems, Budiono et al. [42] finally identified 38 relevant publications with most articles published in the period of 2016–2021. This shows that researchers have recently started to consider the potential of these geothermal systems for sustainable energy exploitation. However, most studies focus on coaxial systems. Although CDG systems are superior to deep coaxial systems in terms of power production and extraction temperature [42], only few papers [43–49] are related to analyzing their heat extraction mechanisms. The systematic work of Budiono et al. [42] is combined with our literature review to provide a comprehensive overview of the conducted studies and the research gap.

In 2018, Song et al. [43] used a synthetic model to evaluate the impact of operational parameters (e.g., flow rate and inlet temperature) on the performance of the CDG system. With respect to the evolution of the production temperature, they distinguished possible decreasing, transition, and stable production scenarios. However, they set up a single stratigraphic structure and assumed the physical properties of water to be constant despite temperature and pressure alteration. In 2018, Sun et al. [44] repeated their study using carbon dioxide as a circulating fluid, and proposed new concepts for the evaluation of the geothermal recovery performance. In 2020, Chen et al. [50] used temperature-dependent equation of state for a limited four months operation period but neglecting the impact of well completion (casings and cement layers) on heat exchange. Yuan et al. [46] evaluated the geothermal energy recovery on an idealized CDG system identifying reservoir thermal conductivity as most important parameter determining the system's energy recovery potential. However, they assumed constant properties for the working fluid without accounting on thermal resistance by convective fluid flow within the wellbores, the steel tube wall, casing, and cement ring. Sun et al. [45] analyzed the geothermal energy production by supercritical CO<sub>2</sub> circulation in CDG systems. They have conducted a sensitivity analysis to

demonstrate the effects of injection parameters, heat transmission fluid, and wellbore properties on the temperature field. However, the short production time (10000 h) and high subsurface temperature gradient (50 °C/km) may lead to an unrealistic estimation of the long-term heat production. Fallah et al. [48] introduced a novel concept of integrating an automated managed pressure operation (MPO) system with a CDG system for scalable power generation. They analyzed the generated thermal power for operation scenarios accounting for vertical depth and horizontal length, open-hole or cased-hole lateral completions, heat insulation or lack thereof of the return flow, and changing pump rates. With depth and horizontal length of the system assumed to be each 7 km and a maximum rock temperature of 250 °C the parametrization precedes current drilling technology. Ghavidel et al. [47] studied the transient heat transfer in CDG systems. Their investigation is different from other reviewed literature as they only focused on heat absorption in the horizontal wellbore. Nevertheless, ignoring the power production in the injection wellbore can result in a notable underestimation of the CDG system's heat extraction potential.

The above-mentioned studies focused on describing the general behavior of CDG systems and suffer from some oversimplifications or unrealistic assumptions. Furthermore, practical proposals to make the CDG system a strong competitor to other conventional geothermal systems are still lacking. The main purpose of this study is to develop novel concepts with relevance to the economic efficiency of CDG systems, which is one of the main barriers to their wider use, based on state-of-the-art simulation techniques:

1. Using thermosiphon effect to decrease the pumping energy, thus reducing the pumping costs. Being not yet numerically analyzed for CDG systems, the magnitude and stability (transient behavior) of thermosiphon flow rate under different geometrical configurations and surface pressure losses will be quantitatively assessed.
2. Valve-controlled thermosiphon flow is suggested by this study to stabilize the extraction temperature and to improve system's longevity. This will result in optimizing flow rate considering thermal power production, extraction temperature stability, and internal energy consumption.
3. Defining new criteria for the calculation of optimum insulation length by addressing a specific absorbed energy. Therewith, the energy absorption of the system is maximized as function of temperature gradient and thermal conductivity.
4. Sectional analysis of power production in CDG systems in vertical and horizontal wellbores are providing quantitative insights for the future design of multi-lateral structures.

To achieve these goals, thermal interactions between different components of the system (i.e., cement, casing, formation, and working fluid) are analyzed. A pressure and temperature-dependent equation of state (EOS) is included to consider the buoyancy force in the thermosiphoning evolution. A fully coupled mathematical and physical model, including continuity, momentum, and energy equations, the EOS, and an analytical lateral heat transfer approach, is employed and presented. Finally, the sectional performance of the system is thoroughly evaluated to avoid production temperature drawdown, which is a severe problem in dealing with closed geothermal systems, and the impact of suggested scenarios on the net generated thermal power, insulation strategy, and pumping energy are further discussed. It should be noted that the CDG system is designed for district heating purposes. Therefore, the word "power" in the next chapters refers to "thermal power", and it is also explicitly mentioned when the system is producing electric power.

## 2. Methodology

### 2.1. Governing equations

To model the CDG systems, three major components, including energy exchange between wellbore and formation, heat transfer in formation, and transient processes in wellbores, should be considered. Fluid flow in tubing undergoes several coupled physical processes, such as pressure change balanced by friction loss, gravity and kinetic energy alteration [51,52], temperature variation due to heat exchange with surrounding formation, and velocity change influencing pressure and temperature fields. In order to appropriately simulate these physical processes, a finite element code, called MOSKITO [53,54], is developed in the MOOSE Framework [55,56] environment to consider such complex physical processes. MOOSE is a multiphysics object-oriented simulation environment that is written in C++. This open-access code can be used for solving a wide variety of partial differential equations.

While the temperature of the circulating fluid may significantly increase, because of its high pressure, the fluid doesn't experience a two-phase state. A non-isothermal transient flow in a pipe is described as [57]:

Continuity equation:

$$\frac{\partial}{\partial t}(\rho) = -\frac{\partial}{\partial z}(\rho v) + m \tag{1}$$

where  $\rho$  and  $v$  are the density and velocity of fluid, and  $m$  is the mass sink/source term in unit volume and unit time.

#### 2.1.1. Momentum equation

$$\frac{\partial P}{\partial z} = \rho g \cos(\theta) \pm \frac{f \rho v^2}{2d} \pm \left( \frac{\partial}{\partial t}(\rho v) + \frac{\partial}{\partial z}(\rho v^2) \right) \tag{2}$$

where  $f$ ,  $g$ ,  $\theta$ ,  $d$  and  $P$  are the friction factor, gravitational acceleration, the inclination of the well, wellbore hydraulic diameter, and fluid pressure, respectively. Depending on flow and gravity directions, the sign of the right hand side (RHS) terms in the momentum equation can change.

#### 2.1.2. Energy equation

$$\frac{\partial}{\partial t} \left[ \rho \left( h - \frac{P}{\rho} + \frac{1}{2} v^2 \right) \right] = -\frac{\partial}{\partial z} \left[ \rho v \left( h + \frac{1}{2} v^2 \right) \right] + \rho v g \cos(\theta) - \frac{q}{A} + Q \tag{3}$$

where  $h$ ,  $q$  and  $Q$  are the enthalpy, lateral heat flow, and heat sink/source terms, respectively.

Based on Eqs. (1)–(3), main variables are the velocity, pressure, and enthalpy of the fluid. This set of coupled partial differential equations (PDEs) will be bounded by transient Dirichlet boundary condition type. To solve these equations, some constitutive relationships/empirical equations, including the viscosity, the density, and the friction factor, are required. The viscosity is calculated by Vogel Equation [58]. An empirical equation of state (EOS) [59] is used to calculate the density as a function of pressure, temperature, and salinity of the fluid (saline water).

The fluid can exchange heat by surrounding structure, including casings, cement layers, and geological formation, through two main mechanisms. The first mechanism is the conductive heat transfer through all layers, and the second mechanism is the convective

heat transfer within a fluid film in the vicinity of the inner tubing wall. In overall, this heat flow can be calculated by:

$$q = 2\pi r_{to} U_{to} (T_f - T_{cf}) \tag{4}$$

where  $r_{to}$ ,  $U_{to}$ ,  $T_f$  and  $T_{cf}$  are the outside radius of the inner tubing, the overall heat transfer coefficient, the fluid temperature, and the temperature at the cement/formation interface, respectively. This lateral heat model updates the temperatures at the interfaces of different layers over time. For a detailed explanation, refer to Willhite [60]. The increase of the casing diameter is accompanied by the enlargement of the heat exchange area leading to losing or absorbing a higher amount of heat. Simulating the thermosiphon flow is one of the main goals. This flow is a self-flowing system driven solely by the density difference at both wellheads due to temperature differences. Therefore, the temperature dependency of the EOS plays a key role since the density monotonically decreases by increasing the temperature. The pressure gradient caused by the density difference acts as the driving force to circulate fluid in the system. However, this pressure gradient should overcome pressure losses in the CDG system (i.e., velocity-dependent) and at surface facilities. Numerical simulation of thermosiphon flow requires special treatment at the boundary. Therefore, a particular type of Dirichlet boundary condition, called velocity postprocessor BC, is designed in this study to automatically calculate the re-injection velocity using wellheads pressure differences reduced by surface facilities pressure loss at each timestep (see chapter 4.2).

### 2.2. Model validation

The presented model on the scale of CDG systems is validated against the results of the study conducted by Song et al. [43]. An identical configuration and parameters, i.e., a flow rate of 70 m<sup>3</sup>/h, an injection temperature of 40 °C, a depth of 3.5 km, and a horizontal extension of 6 km, are assumed. In order to comply with Song et al. [43] study, an EOS with a constant density, ignoring the impact of fluid pressure and temperature, is considered.

Fig. 1 illustrates a comparison of three models for the

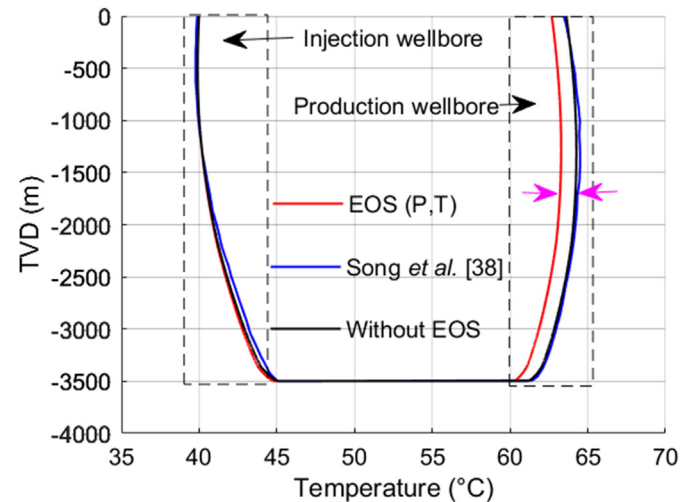


Fig. 1. Comparison between temperature profiles along the system after 20 years of operation. The same style of the reference paper is used for this figure. The pink double arrow shows the variation of calculated temperature in the production wellbore after including the equation of state. The inclusion of the EOS has a negligible impact on the calculated temperature in the injection wellbore.

temperature field. In the first step of validation, all the physical properties of the fluid are assumed to be constant despite temperature and pressure changes. The obtained result perfectly agrees with the results of Song et al. when the simulation is conducted without EOS. Nevertheless, the considerable variations of pressure and temperature in this deep geothermal system can affect the fluid properties. Therefore, in the second step, the temperature and pressure-dependent EOS is used to account for the alterations of density, viscosity, and specific heat capacity. The inclusion of the EOS has no notable impact on the computed temperature profile in the injection wellbore. However, it reduces the calculated temperature in the production wellbore ( $\approx 1\text{ }^\circ\text{C}$ ) as the fluid experiences larger pressures and temperatures in this section of the system.

### 2.3. Numerical modeling

In the present study, the CDG system is supposed to provide a continuous supply for district heating purposes over the whole year, thus neglecting possible recovering periods. The geometrical configuration of the system comprises of three sections (Fig. 2): I) a vertical injection well, II) a horizontal well, and III) a vertical production well. The vertical wells are relatively deep, and they are connected at the bottom hole through the horizontal well, which is relatively long. The vertical wells (sections I and III) are cased to avoid subsurface contamination and maintain wellbore stabilities, while the horizontal extension (section II) is directly exposed to hot formation to maximize energy absorption. It is supposed that the injection of some chemicals seals the lateral area around section II [41]. The heat exchange in sections I and III is regulated by the number of layers around the wellbore, their thicknesses, fluid velocity, pipe roughness, and thermophysical properties of casing, cement, formation, and circulating fluid. However, depending on the pressure difference between circulating fluid and the surrounding environment, we may have lateral inflow or outflow through section II. This direct exposition is necessary since casing the horizontal section, like the lower section of vertical wellbores,

increases the total thermal resistivity by 40%.

A reference model with specific configuration and parameters is introduced below. the configuration and parameters of the reference model are preserved throughout this study unless otherwise noted.

#### 2.3.1. Reference model

In the reference model, both the vertical depth,  $\Delta z$ , and the horizontal length,  $\Delta l$ , are 4 km, as shown in Fig. 2. This figure also demonstrates the wellbore diameters, which ranges from 8  $\frac{3}{8}$ " (section II) to 22" (the upper part of section I), as well as casings arrangements. The roughnesses of sections I, II, and III are  $10^{-4}\text{ m}$ ,  $2 \times 10^{-4}\text{ m}$ , and  $10^{-4}\text{ m}$ , respectively [61]. The formation surrounded the system consists of two geological units with a depth of 2 km each. The thermal conductivities of the upper and lower layers are 2 and 3  $\text{Wm}^{-1}\text{K}^{-1}$ , respectively. The underground subsurface temperature gradient is assumed to be 30  $^\circ\text{C}/\text{km}$ , and the temperature at the surface is 10  $^\circ\text{C}$ . All thermo-physical properties of the cement layer, casing, and formation are shown in Table 1.

The initial temperature of the circulating fluid is assumed to be the same as the ambient formation temperature considering a thermal equilibrium between the residual fluid and the surrounding formation. The initial pressure condition is hydrostatic. Moreover, Dirichlet boundary conditions with fixed values are applied at the injection point. A constant salinity of 0.25 molal is considered while, using Dirichlet BCs, the injection temperature, pressure, and flow rate are set at 10  $^\circ\text{C}$ , 100 kPa, and 5 L/s, respectively.

A sensitivity analysis for three spatial discretizations ( $\Delta x = 14\text{ m}$ ,  $\Delta x = 11\text{ m}$ , and  $\Delta x = 7\text{ m}$ ) was conducted to confirm that the solution is mesh-independent. Evaluation of pressure and temperature fields over the length of the wellbores revealed the negligible impact of implemented mesh sizes on the results. The maximum relative variation of pressure and temperature values is below  $6 \times 10^{-4}\%$  when changing the mesh size from 7 m to 14 m. Even though, the mesh size of 14 m is acceptable for this study, the mesh size of 7 m was used due to the reasonable computational cost. The total simulation time is 100 years which time steps

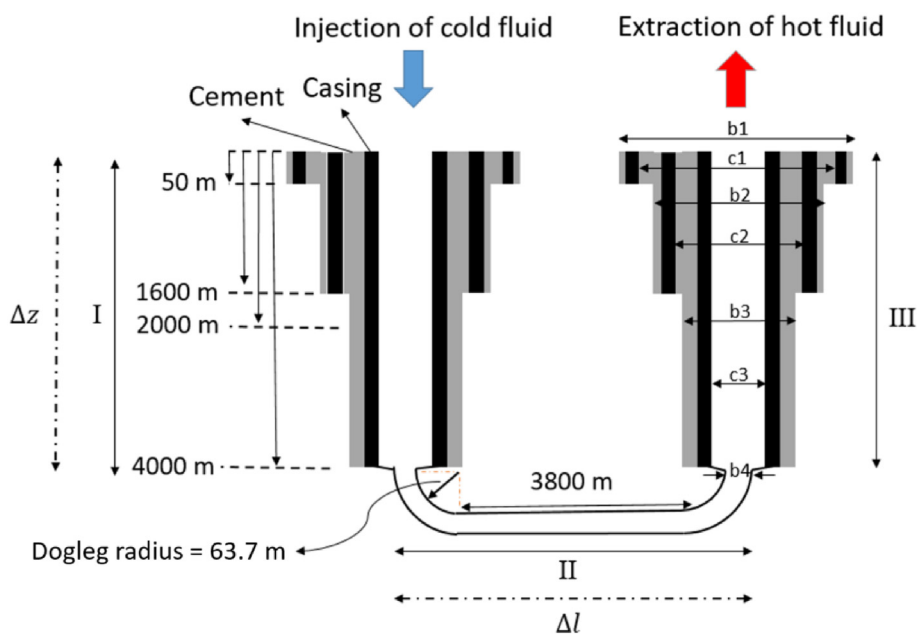


Fig. 2. Schematic illustrating geometrical features of the reference model.  $b_1, b_2, b_3,$  and  $b_4$  stand for borehole diameters where the wellbore structure is in direct contact with the formation.  $c_1, c_2,$  and  $c_3$  also represent casings' inner diameters. ( $b_1 = 0.5588\text{ m}, c_1 = 0.473075\text{ m}, b_2 = 0.4318\text{ m}, c_2 = 0.346075\text{ m}, b_3 = 0.31115\text{ m}, c_3 = 0.244475\text{ m}, b_4 = 0.212725\text{ m}$ ).  $\Delta z$  and  $\Delta l$  show the depth of vertical wells and total horizontal length, respectively. The horizontal section is directly exposed to hot formation.

**Table 1**  
Thermo-physical properties of formation, casing, and cement layer.

Formation density	Formation heat capacity	Formation thermal conductivity (upper layer)	Formation thermal conductivity (lower layer)	Cement thermal conductivity	Casing thermal conductivity	Subsurface temperature gradient	Ground surface temperature
$\text{kg} \cdot \text{m}^{-3}$	$\text{J} \cdot \text{kg}^{-1} \cdot \text{K}^{-1}$	$\text{W} \cdot \text{m}^{-1} \cdot \text{K}^{-1}$	$^{\circ}\text{C} \cdot \text{km}^{-1}$	$^{\circ}\text{C}$			
2400	1000	2	3	0.7	100	30	10

gradually increase from 100 s to one month. While the operation period of 100 years is much longer than the lifetime of conventional geothermal systems (i.e., 30 years), evaluation of the ratio of generated power to the total length of the wellbores revealed that this system requires a long payback period. Additionally, the assessment of the system's long-term performance helps to compare its longevity against other geothermal systems. This long operation period is also suggested by some other companies working on this system [41]. Consequently, all the casing, cement layers, insulation, and pumping should efficiently work for a long period which is a serious issue while operating with this system.

2.3.2. *Insulation strategy for production well*

Proper insulation of production wellbore is a key aspect of designing CDG systems. The main purpose of insulation is to prevent heat loss at areas in which the temperature of the circulation fluid is higher than those of surrounding areas. However, temperature alteration of the fluid and its adjacent formation leads to the continuous change of insulation length. Since the length of the insulation layer cannot vary over time, this length should be properly estimated to minimize heat loss and to be practical for construction. Hence, the total absorbed energy in each section should be calculated to determine zones in which the total exchanged energy possesses a negative value (i.e., energy loss). The total absorbed energy per meter (TAEM) for different sections after 100 years of operation is plotted in Fig. 3.a. The TAEM value of each section depends on lateral exchange area, total thermal conductivity, and temperature difference between circulating fluid and surrounding area ( $\Delta T$ ) as per Eq. (4). Positive values reflect heat absorption from the surroundings, while negative values yield heat losses to the surrounding. The jumps of the TAEM at points  $\beta$  and  $\zeta$  (in sections I and III, respectively) originate from the alteration of the formation thermal conductivity at the depth of 2 km as introduced in the previous section. Similarly, the jump of the TAEM at point  $\alpha$  is related to the changes of casing and cement layers, as per

Fig. 2, leading to the reduction of the total thermal resistivity.

Since the lateral exchange area is constant in each section (I, II, and III) and the jumps are explained above, the overall trend of the TAEM is mainly dependent on  $\Delta T$ . In section I,  $\Delta T$  grows by the depth leading to increasing of the TAEM. However, the temperature of the circulating fluid approaches the surrounding temperature along section II, leading to the reduction of  $\Delta T$  resulted in the decline of the TAEM. Similarly, this trend is observed in section III, with the exception that the TAEM changes the sign (from positive to negative) in this section. Point  $\gamma$  in Fig. 3.a indicates that the circulating fluid is hotter than the surrounding formation, and the fluid is losing heat from this point up to the extraction point. To avoid the cooling of the circulating fluid, proper insulation of section III is necessary from point  $\gamma$  upward as illustrated in Fig. 3b. However, the insulation arrangement in Fig. 3.c is considered in this study to prevent severe complexity in practical well design and drilling plans. The thermal conductivity of the insulation material (urethane fiberglass) is  $\lambda = 0.021 \text{ Wm}^{-1}\text{K}^{-1}$  [62]. This insulation configuration prevents 50 GJ/m heat loss at the upper part of section III. It is worth mentioning that the insulation length mainly depends on operation duration and production flow rate. Moreover, operating in highly conductive geothermal fields with a large subsurface temperature gradient may increase the optimum length of the insulation layer.

3. Evaluation of the CDG system long-term behavior

3.1. Impacts of flow rates on the produced temperature and energy

In this chapter, the system behavior for different flow rates of 1 L/s, 5 L/s, and 10 L/s are evaluated assuming the reference model conditions (Fig. 4).

Fig. 4 shows the impact of flow rate on the behavior of production temperature over time. The immediate rise of the extraction temperature in the first few days is due to the residual hot fluid

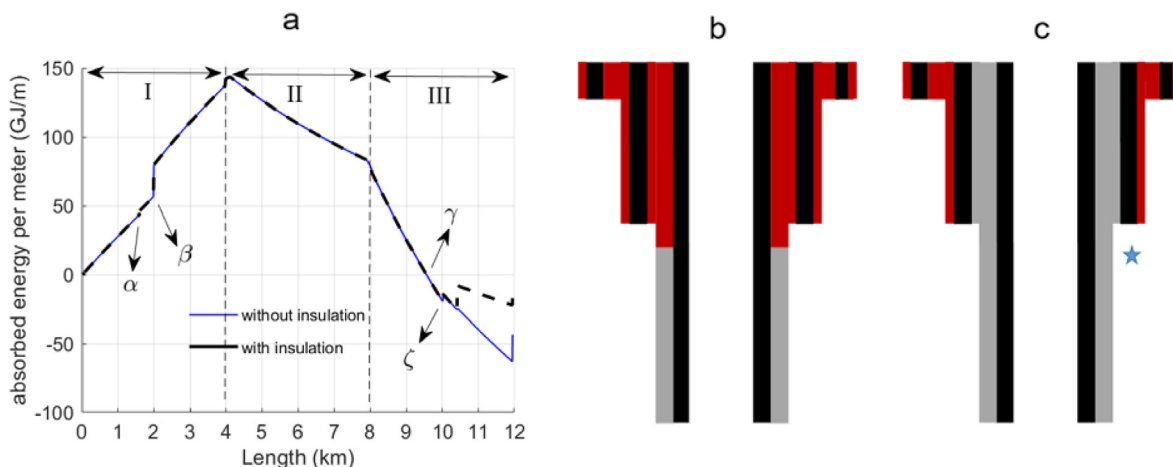


**Fig. 3.** a) Impact of insulation of production wellbore on the total absorbed energy per meter of the CDG system after 100 years of operation (insulation layer is highlighted by red color). The corresponding lines for the presented cases overlap up to the insulation section. b) Ideal insulation of production wellbore c) practical insulation of production wellbore.

displacement. After this short period, the production temperature tends to decrease (Fig. 4, flow rate = 10 L/s and flow rate = 5 L/s), which is a well-known behavior in closed geothermal systems. The rapid decline in the production temperature is the major challenge of the CDG system. However, to guarantee the reliability of the system for district heating purposes, a production temperature of at least 80 °C at a meaningful flow rate is required, which is further analyzed in the following. The system's thermal performance is strongly dependent on flow rate due to the heat exchange rate between the surrounding formation and the circulating fluid. Accordingly, the reduction of the circulating fluid velocity results in reaching a higher temperature along the injection and horizontal wells (sections I and II) but thermal huge temperature loss along the production well (section III). Fig. 5 illustrates this behavior for these sections at different flow rates and timings.

The duration of heat exchange for a given volume of fluid is longer at smaller flow rates, which plays a key role in regulating the extracted/lost heat in each section of the system. Over time, the fluid temperature in sections I and II is decreasing regardless of the flow rate. In section III, a similar trend is observed except for the flow rate of 1 L/s, when a hotter fluid enters the production wellbore, and it has a longer time to exchange heat with the surrounding formation. Therefore, the circulating fluid loses a lot of energy, represented by a notable temperature drop in the production wellbore. For this flow rate, the circulating fluid heat loss causes the surrounding formation around section III to warm up over time, leading to prevention of the mentioned temperature drop and continuous production temperature rise, as shown in Fig. 4. In the other flow rates, such an effect is not observed as 1) the fluid velocity is higher, so the heat loss is lower in section III, and 2) the circulating temperature is closer to the surrounding formation around section III because of low heat gain in section I and II (due to high fluid velocity). This reveals the importance of the heat exchange duration. The energy loss may contradict the idea of maximizing power generation. However, it is useful when a high stable extraction temperature is required for operation. It is also noteworthy that sometimes the increase of extraction temperature compensates for the decrease of flow rate. Therefore the generated power doesn't change significantly.

Aside from the heat exchange duration discussed above, the

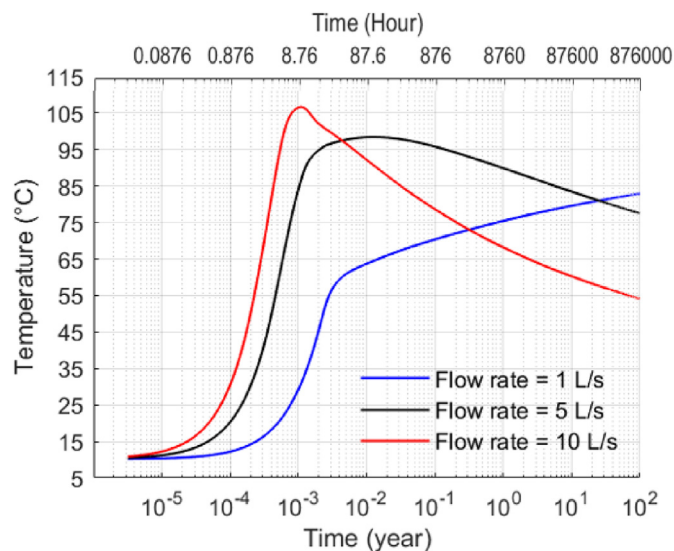


Fig. 4. Extraction temperatures over time for different flow rates. The short-term behavior of the extraction temperature is caused by the displacement of residual hot fluid, while its long-term behavior is controlled by the lateral heat exchange.

flow rate can remarkably influence the convective heat transfer factor leading to the variation of the heat exchange rate. This factor is a function of the Reynolds number, friction factor, and Nusselt number, which are all functions of the circulating fluid velocity. For instance, the convective heat transfer factor in the case of the flow rate of 1 L/s takes values between 91.6 W/m<sup>2</sup>•K and 164.5 W/m<sup>2</sup>•K, while it ranges between 577.8 W/m<sup>2</sup>•K and 932.75 W/m<sup>2</sup>•K for the flow rate of 10 L/s. Therefore, the interplay between the heat exchange duration and the heat transfer factor, which are strongly functions of the fluid velocity at each section (I, II, and III) and the overall system's flow rate, is the key factor to stabilize the production temperature over time and maintain the longevity of the CDG system.

The produced energy of the reference model can range between 1 PJ and 6 PJ for the simulated flow rates (Fig. 6). The generated power and energy production depend on flow rate and the temperature difference between injection and extraction points. As mentioned before, the increase of the flow rate is associated with the extraction temperature decrement. However, there is not a linear relation between variations of extraction temperature and flow rate. As shown in Fig. 6, the increase of the flow rate from 1 L/s to 5 L/s can remarkably enhance the cumulative absorbed energy over time. It means the increases of flow rate prevailed over the reduction of extraction temperature. However, further increase of the flow rate from 5 L/s to 10 L/s doesn't considerably enhance the energy absorption. It indicates that the severe reduction of the extraction temperature doesn't allow for a significant improvement of energy absorption. Consequently, the decrease of extraction temperature, generated power, and energy absorption rate are the main barriers to the increase of the operating flow rate.

To better evaluate the total extracted energy in Fig. 6, a sectional (I, II and III) performance of a CDG system is illustrated in Fig. 7. Fig. 7a shows that the extracted heat in section I is mainly wasted in section III (almost mirrored curves around the power of zero). However, this lost heat in all cases is reduced over time since the warm up bubble around section III get bigger and hotter (it is also explained in Fig. 5). Interestingly, the total net power curve in Fig. 7b for each flow rate mainly mimics the power behavior of section II which is shifted by the difference of the obtained powers in section I and III. Therefore, the extracted heat in section II and preventing heat loss in section III are of paramount importance in the production temperature sustainability and power longevity.

### 3.2. Impacts of wellbore diameter on the produced power

The friction loss is proportional to the circulating fluid velocity. Hence, reducing wells diameters increases frictional loss, assuming the same flow rate. The following sensitivity study is performed: Case 1 is devised by subtracting 4 " from the wellbore diameters of the reference model, while the wellbore diameters of case 2 are 4 " larger than those of the reference model. The rest parameters are the same as of the reference model.

As exhibited in Fig. 8a and Fig. 8b, altering the wellbore diameters does not have a considerable impact on the generated power. Wellbore diameter increment is associated with the enlargement of the lateral heat exchange area. Additionally, the heat exchange duration and the convective heat transfer factor change. These changes and enlarged area are in the favor of the case 2 resulted in higher produced power. Nevertheless, this is a proof of the complex behavior of the system and the demand for an advanced mathematical and physical model. In conclusion, regardless of the negligible changes in the produced power, the feasibility of the drilling cost reduction by decreasing the wellbore diameters is showcased in this section.

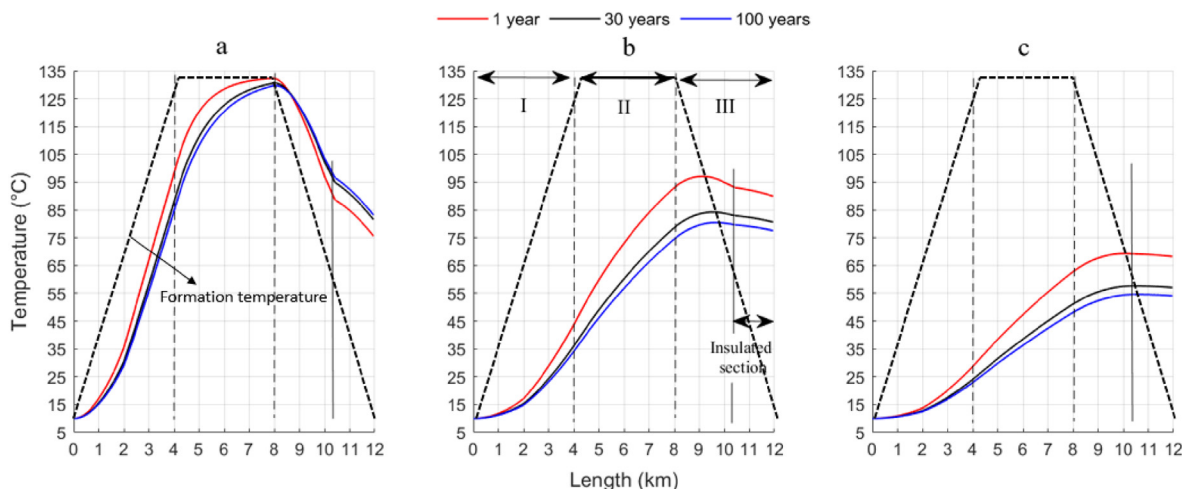


Fig. 5. Temperature distribution in each section of the system (I, II, and III) for a) flow rate = 1 L/s b) flow rate = 5 L/s c) flow rate = 10 L/s. The difference between temperature profiles along the wellbores and formation temperature (dashed line) can be used for the determination of the locations requiring insulation.

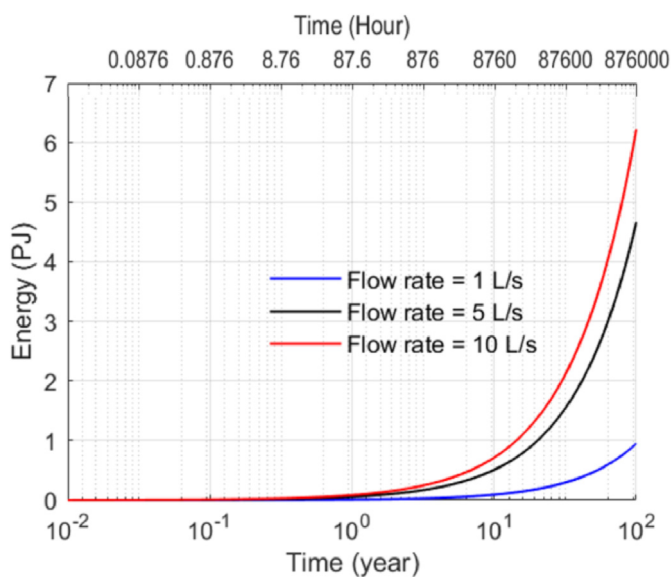


Fig. 6. Cumulative extracted energy over time for different flow rates. After 100 years of operation, the absorbed energy with the flow rate of 10 L/s is 6 times of heat absorption with the flow rate of 1 L/s.

### 3.3. Impacts of geometrical configurations on the produced temperature

As discussed before, the main objective of this study is to better assess the CDG system for district heating purposes. However, the feasibility of the CDG system to be utilized for electricity production is also evaluated in this system. Hence, two cases are designed here to testify the possibility of long-term hotter produced temperature (>100 °C) compared to the case of district heating (>80 °C). These scenarios are: 1) the injection temperature of 70 °C, and 2) increasing the depth and the length of the system. For the first case, the reference model is used and only the injection temperature increased from 10 °C to 70 °C. For the second case, all sections' length and depth are incremented by 1 km compared to the reference model. Hence, sections I and III are 5 km deep, and section II is 5 km long.

As depicted in Fig. 9, even with the increase of the injection

temperature (case 1), the extraction temperature is still lower than 100 °C. Meanwhile, raising the injection temperature brings on a lower generated power. However, case 2 (enlarging the CDG system geometry) is successful in maintaining the produced temperature above 100 °C over a period of one century. This success is due to accessing a hotter formation in the depth of 5 km. It is noteworthy that decreasing the flow rate leads to enhancing the produced temperature (as shown in Fig. 4) while the generated power reduces.

## 4. Thermosiphon flow assessments

The temperature difference across a CDG system, particularly wellhead, leads to a density difference since the circulating fluid EOS is temperature-dependent. Consequently, the existence of a heavier fluid in the injection well (section I) compared to a lighter fluid in the production well (section III) triggers the fluid circulation known as thermosiphon flow. This phenomenon can significantly decrease the required pumping power for the fluid circulation in a CDG system, and it can potentially make the system independent of an external power grid.

Before operation, the temperature field was undisturbed with temperature profiles of injection and production wells being identical. An initial forced circulation is required to displace the residual fluid in the system, to create a temperature difference between sections I and III, and to trigger the thermosiphon flow. Accordingly, an initial period of ten days forced, pump-driven circulation was taken to establish the temperature contrast between the wellheads, necessary to trigger thermosiphoning. This thermosiphon flow is calculated by applying the “velocity post-processor boundary condition” (see Chapter 2.1) taking the reference model as basis. The sensitivity analysis accounts for various factors that could impact the resistive forces on fluid circulating, such as surface pressure losses and system geometry.

### 4.1. Impacts of surface facilities pressure losses

The thermosiphon effect in CDG systems overcome pressure losses in both subsurface wells and surface facilities (e.g., heat exchangers, piping, etc.). The frictional pressure loss of the surface facilities,  $\Delta P_s$ , is incorporated as a bulk pressure loss ranging from 0 kPa to 900 kPa. Fig. 10 illustrates that a thermosiphon flow rate of  $Q_{TS} > 11$  L/s would be yielded after 100 years of the production even

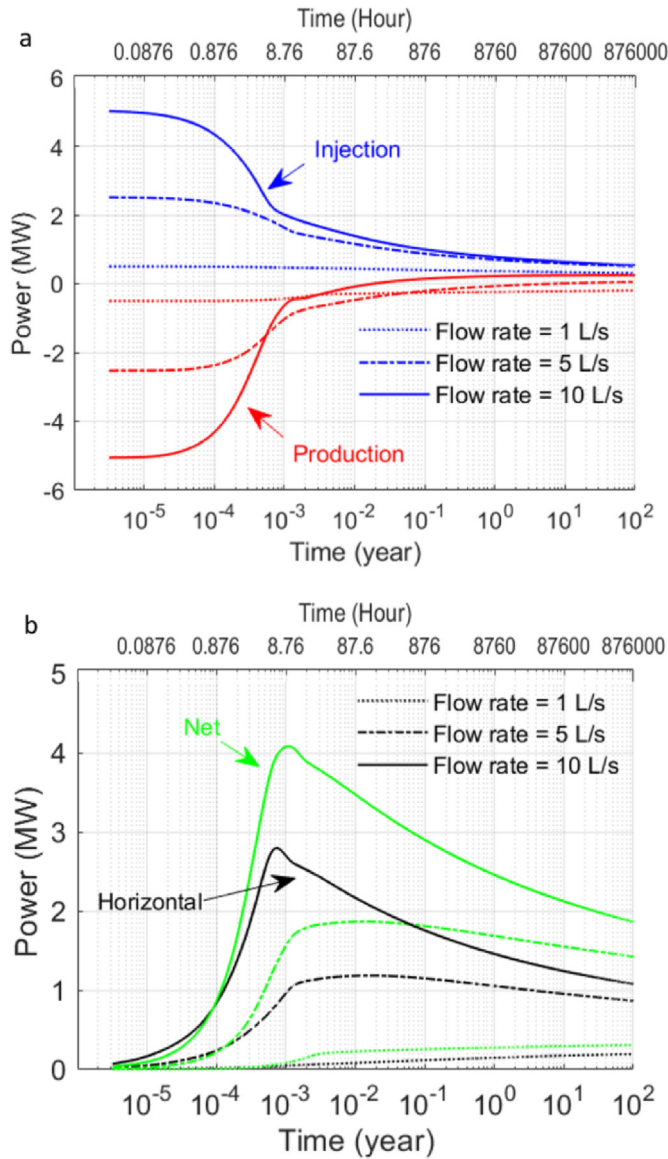


**Fig. 7.** Flow rate impact on: a) generated powers in vertical wells b) net generated power and produced power in the horizontal section over time. For each flow rate, the variation of net power over time is like the transient behavior of produced power in the horizontal wellbore.

for the extreme case of  $\Delta P_s = 900$  kPa. Over the lifetime of the system, although the temperature and density contrasts between the wellheads at sections I and III reduce, the thermosiphon effect will not weaken significantly. It is noteworthy that all operating flow rates assumed in Chapter 3 (i.e., 1 L/s, 5 L/s, and 10 L/s) are smaller than the lowest calculated thermosiphon flow rate of 11 L/s.

The optimum flow rate for the operation depends on power production, extraction temperature, and pumping power. The following assessment of thermosiphoning presumes that the pumps are shut-off and no pumping is required to circulate the fluid in the system, thus reducing the corresponding operation cost to zero. In the considered range of 1–10 L/s (Fig. 7) the produced thermal power increases with flow rate. Therefore, extraction temperature is the only limiting factor when determining an optimum valve-controlled flow rate. For example, operating with the valve-controlled flow rate of 5 L/s leads to the extraction temperature of  $\approx 80$  °C after 100 years of operation (Fig. 4).

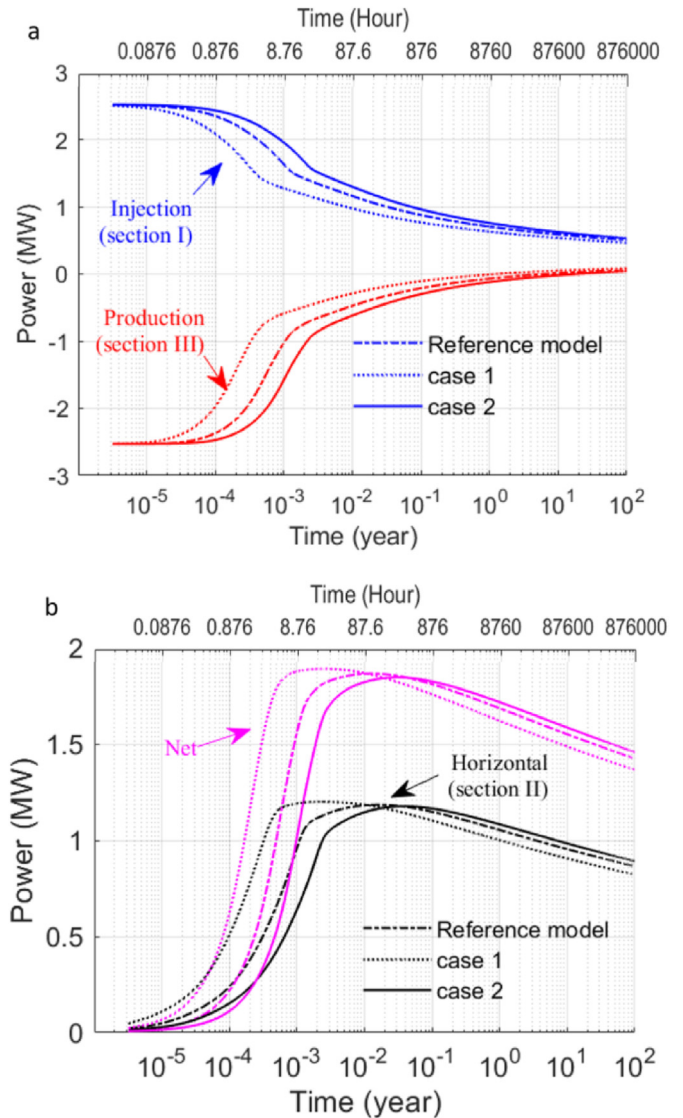


**Fig. 8.** Impact of wellbore diameter (case 1–4" smaller and case 2–4" larger diameter than the reference model) on: a) generated powers in vertical wells b) net generated power and produced power in the horizontal section over time.

#### 4.2. Impacts of wellbores diameters and geometrical configurations

Similar cases of chapter 3.2 are repeated for the simulation of the thermosiphon flow with  $\Delta P_s = 900$  kPa (Case 1 is devised by subtracting 4" from the wellbore diameters of the reference model (Fig. 2), while the wellbore diameters of case 2 are 4" larger than those of the reference model). As illustrated in Fig. 11, the case 2 setup generates a thermosiphon flow being twice as high as case 1. Nevertheless, the obtained QTS for case 1 is still sufficient to produce the desired TTS since the flow rate for the Min TTS = 80 °C should be less than 5 L/s (Fig. 4). Consequently, case 1 is economically beneficial due to the reliance of drilling cost on wellbore diameter (i.e., smaller wellbore diameter significantly reduces drilling expenses).

Irrespective of the wellbore diameter, the influence of the depth and horizontal length of a CDG system on the thermosiphon flow should be investigated. Hence, two systems with a total length of 12 km are considered to evaluate the impact of geometrical configurations on the thermosiphon flow rate. System 1 owns the same

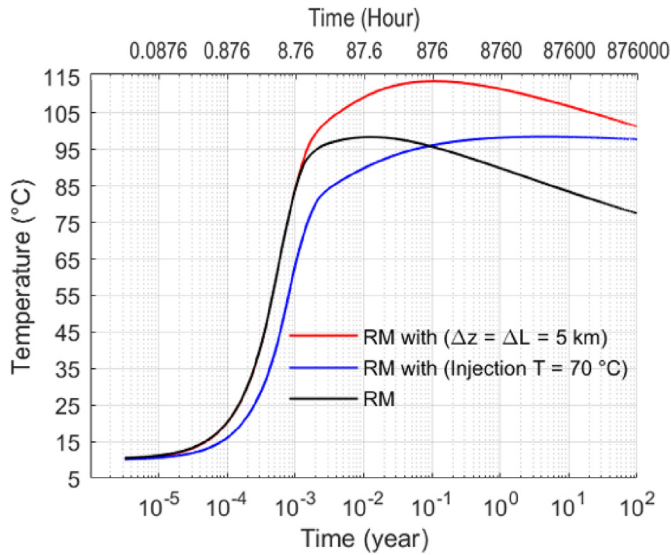


**Fig. 9.** Comparison between the impacts of injection temperature increment and system enlargement ( $\Delta z = \Delta l = 5$  km) on the extraction temperature of the reference model (RM and T stand for reference model and temperature, respectively). System enlargement is superior to the injection temperature increment to enhance the extraction temperature.

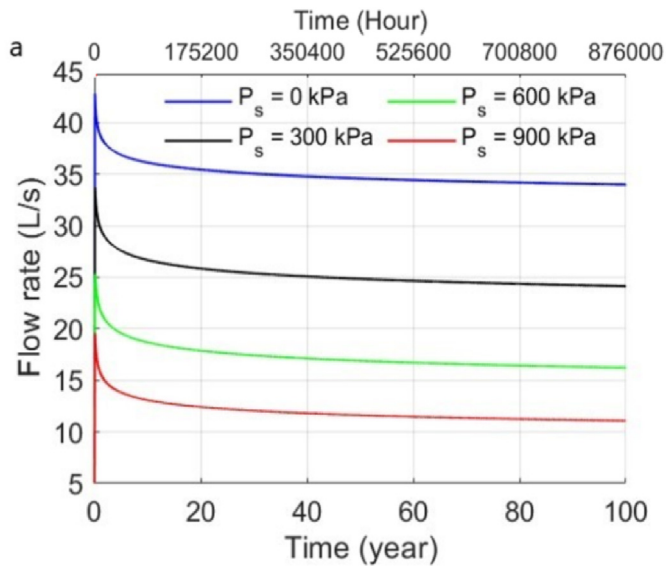


**Fig. 10.** Impact of pressure loss at surface facilities on the thermosiphon flow rate over time. In all the cases, the thermosiphon flow rate is stable over time. Even in the worse case, with the surface pressure loss of 900 kPa, the thermosiphon flow rate is higher than 11 L/s.

geometry as the reference model, while in system 2, the depth of sections I and III and the length of section II are 3 and 6 km, respectively. All other parameters are the same as the reference model. As depicted in Fig. 12, it is more beneficial to deepen the system rather than extending it horizontally because the deeper system gets access to hotter formation for the same subsurface temperature gradient. Operating With a system possessing a longer horizontal section enhances the heat extraction surface and increases the temperature difference between vertical wellbores. However, in the case of a deeper system, not only the heat exchange surface is more extensive, but also the system gets access to hotter formation for the same subsurface temperature gradient.

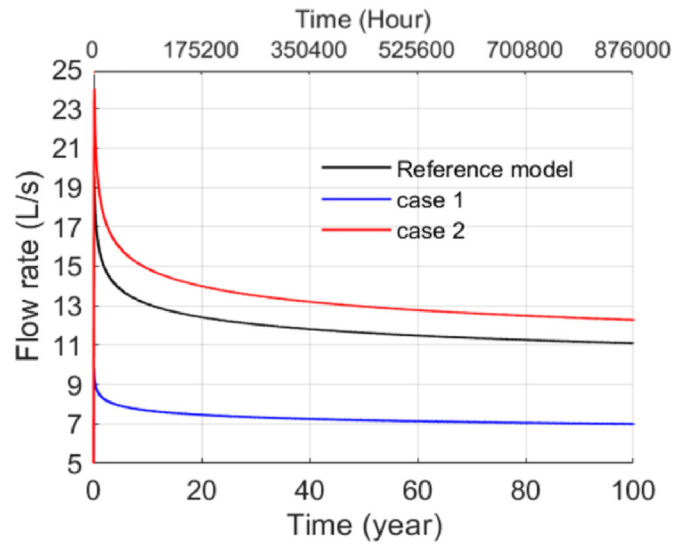


**Fig. 11.** Impact of wellbore diameter on the thermosiphon flow rate over time (case 1 = 4" smaller and case 2=4" larger diameter than the reference model). The case 2 setup (larger diameter) generates a thermosiphon flow being twice as high as case 1 (smaller diameter).

Therefore, the thermosiphon flow rate increases significantly. While the thermosiphon flow rate is mainly influenced by the depth of the system, the magnitude and behavior of total generated power depend on the generated power in the horizontal wellbore (Fig. 7). Hence, it is not reasonable to ignore the importance of horizontal extension of the system. It is worth mentioning that in a real situation, the drilling costs/risks of both vertical and horizontal wellbores should also be taken into account to design the system appropriately.

### 4.3. Controlling thermosiphon flow

Operation with a high flow rate results in a low extraction temperature. As shown in Fig. 10, the lowest thermosiphon flow rate ( $Q_{TS} \approx 11$  L/s) is calculated for the highest surface pressure loss (900 KPa). Nevertheless, even for this small flow rate, the average extraction temperature is approximately 50 °C (Fig. 13a). It means the thermosiphon flow rate should be restricted to achieve a higher extraction temperature ( $T_{TS}$ ). In other words, the thermosiphon flow rate should be controlled by a valve to produce hotter fluid, which is extremely important for dimensioning of a CDG system and identifying economically beneficial operational scenarios.

As an example, a valve-controlled thermosiphon flow rate of 6.6 L/s for the case of ( $\Delta P_s = 900$  KPa) results in producing hot fluid with a temperature of higher than 70 °C over the project lifetime of a century (Fig. 13b). In this case, the control of the thermosiphon flow rate results in producing hot fluid at a meaningful flow rate and reasonable extraction temperature over a long period.

## 5. Discussion

In the last chapters, the CDG system's behavior for several operational and geometrical cases and the feasibility of the thermosiphoning are extensively presented. In this section, a CDG system is further evaluated and discussed to 1) maximize the generated power, 2) to decrease relative drilling cost, and 3) to enhance thermosiphon flow.

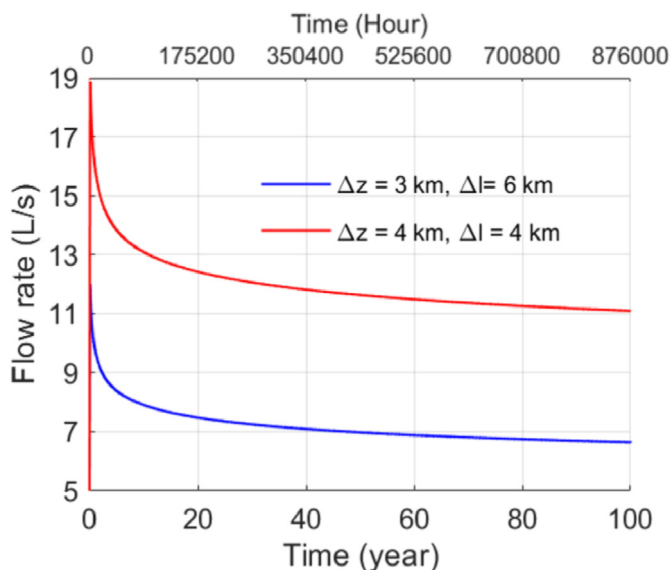


Fig. 12. Thermosiphon flow rates for various CDG configurations over time ( $\Delta z$  = depth of vertical wellbores,  $\Delta l$  = length of horizontal section). The total length of both systems is 12 Km.

5.1. The CDG system geometry

Decreasing the total length and wellbore diameters of a CDG system certainly result in a considerable reduction of relative drilling costs. Based on results, the reduction of wellbores diameters has negligible impacts on the generated power, as well as a sufficient flow rate can still be generated in the case of the thermosiphon flow. However, accessing a hotter underground for the horizontal section through a deeper system is extremely important since the net generated power mimics the behavior of the generated power in the this section. Meanwhile, different geometrical configurations should be individually analyzed since it is significantly dependent on geological settings which is unique for every project.

Operating in a region with a higher subsurface temperature gradient is associated with a higher production temperature and generated power. By assuming the reference model conditions, three models with different subsurface temperature gradients of 30, 35, and 40 °C/km are simulated. By increasing the subsurface temperature gradient of the reference model, the circulating fluid temperature is higher at the end of section II (Fig. 14). However, the fluid loses/gains in section III higher heat compared to the cases with a lower subsurface temperature gradient. Therefore, this leads to the fact that TAEM (as explained 2.3.2) changes in section III at the same location in all cases resulted in the independence of the insulation layer's length from the subsurface temperature gradient.

Similarly, three models (case 1, 2, and 3) with different thermal conductivities of 2, 3, and 4 W m<sup>-1</sup>K<sup>-1</sup> for the lower formation are simulated by assuming the reference model conditions. In contrast to the subsurface temperature gradient, formation thermal conductivity has a major impact on the length of the insulation layer (Fig. 15). Operating in a region with a high thermal conductivity necessitates extending the insulation layer. Therefore, geological settings, particularly thermal conductivity, have direct impacts on the insulation layer length, which influences the drilling costs.

In general, decreasing the fluid velocity in the production well (section III) and achieving a higher temperature of the circulating fluid at the end of the horizontal well (section II) increase the

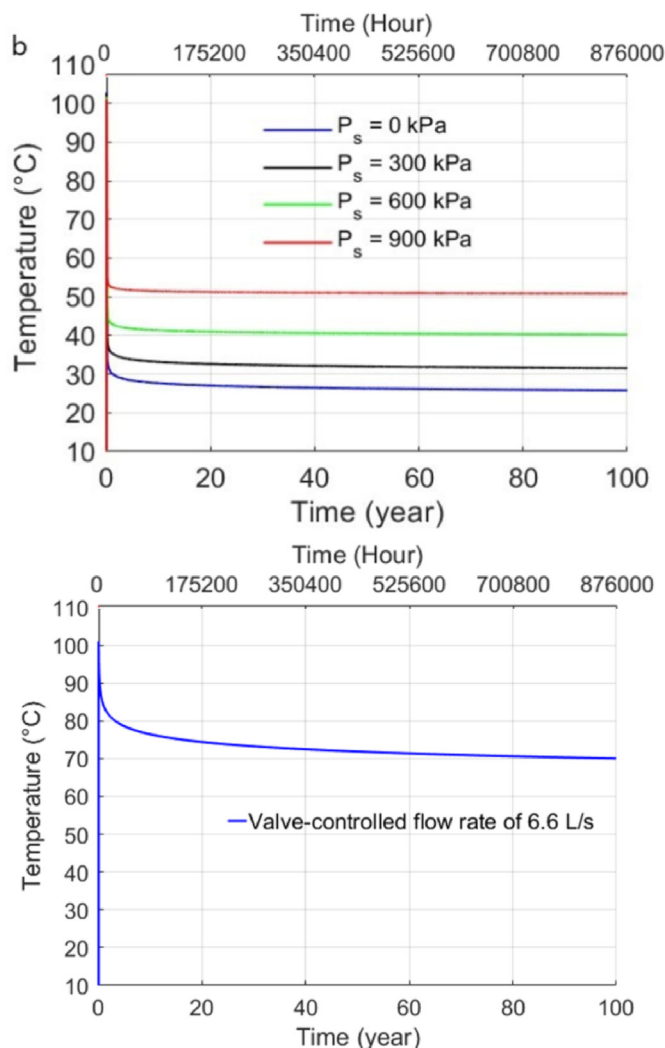


Fig. 13. a) Corresponding extraction temperatures for the flow rates of Fig. 10 and b) calculated extraction temperature for the valve-controlled flow rate of 6.6 L/s and surface pressure loss of 900 kPa.

insulation layer's length. Accordingly, the following scenarios increase the temperature of the fluid entering the production wellbore and extend the length of the insulation layer:

- o Increasing inlet temperature
- o Decreasing flow rate
- o Deepening the system
- o Extending horizontal section

5.2. System's longevity and sustainability

Commonly, the scenarios that maximize heat loss in the production wellbore can improve the system's longevity. Although the heat loss in section III decreases the rate of heat extraction from the system, it warms up the surrounding section III, leading to the stabilization of the production temperature. For example, raising the inlet temperature can prevent the production temperature drop over time (Fig. 9), but it decreases the net generated power dramatically.

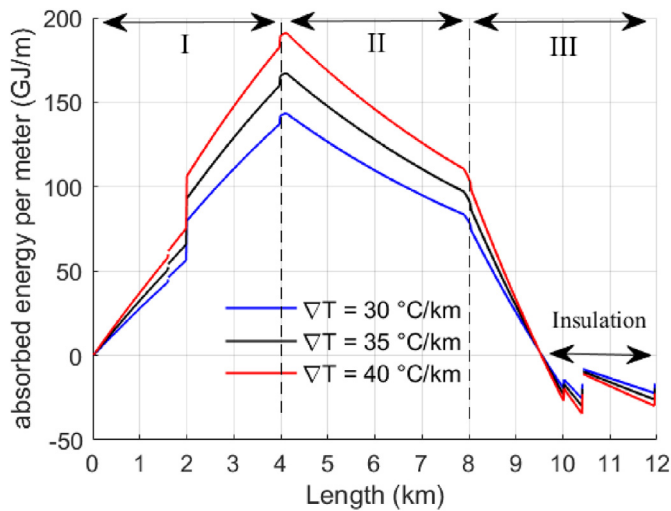


**Fig. 14.** Impact of subsurface temperature gradient on the cumulative absorbed energy per meter of the CDG system after 100 years of operation. The locations with negative absorbed energy should be insulated to avoid heat loss. The jumps of the absorbed energy at different points are explained in chapter 2.3.2 and Fig. 3.

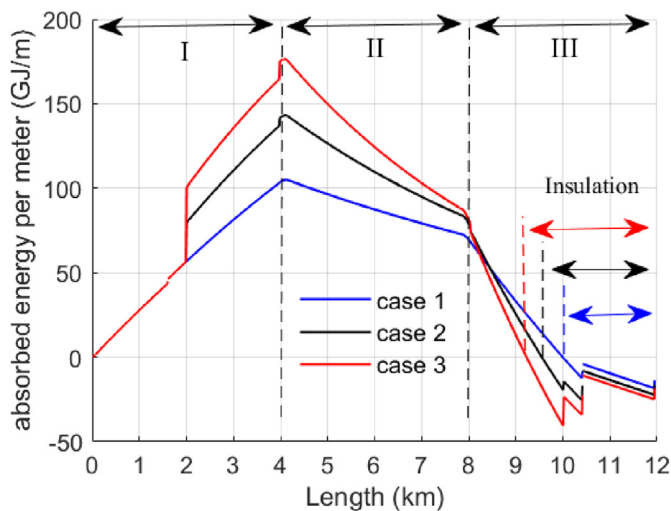


**Fig. 15.** Impact of formation thermal conductivity on the total absorbed energy per meter of the CDG system after 100 years of operation. Thermal conductivity of the upper layer is  $2 \text{ W m}^{-1}\text{K}^{-1}$ , and Thermal conductivities of the lower layer for case 1, 2, and 3 are 2, 3, and  $4 \text{ W m}^{-1}\text{K}^{-1}$ , respectively. The locations with negative absorbed energy should be insulated to avoid heat loss. The jumps of the absorbed energy at different points are explained in chapter 2.3.2 and Fig. 3.

**5.3. Thermosiphoning and drilling costs**

A proper design of the CDG layout significantly enhances the thermosiphon flow. However, it may increase the drilling costs concurrently. For instance, deepening the CDG system, extending the length of the horizontal well, and enlarging wellbore diameters enhance the thermosiphon flow (Figs. 11 and 12). Nonetheless, all of these cases result in additional drilling costs. Additionally, the generated thermosiphon flow in this study was always greater than the optimal flow rate required for district heating purposes. For the district heating, both high extraction temperature and high generated power are required. The results of our simulation (Figs. 4 and 7) revealed that the flow rate of roughly 5 L/s yields approximately 1.5 MW power with the extraction temperature of 80 °C. In the other hand, more effective insulation also results in increasing

the thermosiphon flow. Therefore, it is more beneficial to better insulate the system rather than enlarging it to achieve higher thermosiphon flow.

**5.4. Production pressure and operational energy**

As explained in chapter 3.3, extending the total length of the system (case 2 in chapter 3.3) is more beneficial than re-injection of hot fluid to enhance the production temperature and generated power (Fig. 9). Fig. 16 proves that case 2 is also advantageous for increasing the pressure gradients between wellheads, and it can enhance the thermosiphon flow. This is highly important when the operating flow is higher than the thermosiphon flow leading to the reduction of the operational energy (~cost) because of the less required pumping power.

**5.5. Production well diameter impacts**

Changing wellbore diameter considering a constant flow rate leads to the increase/decrease of the circulating fluid velocity, which influences the heat exchange rate dramatically, as explained in section 3.1. Based on the results, it is expected that larger wellbore diameters in sections I and II and a smaller wellbore diameters in section III should improve the performance of a CDG system. To testify this expectation, the reference model is modified by subtracting 4'' from the diameters in section III, while the diameters of sections I and II remained unchanged, and the flow rate of 1 L/s is simulated. Fig. 17 and Fig. 18 show the impact of decreasing production wellbore diameter on the extraction temperature/pressure. As expected, the production temperature increased about 5 °C, but the production pressure is surprisingly enhanced even considering a higher friction loss due to a higher velocity in section III. Production temperature enhancement escalates the mean temperature difference and density contrast between vertical wells (sections I and III). The difference between weights of vertical water columns increases the extraction pressure, while the pressure loss due to friction reduces it. By decreasing the production wellbore diameter, the larger density contrast prevails the incremented friction loss. Consequently, the extraction pressure enhances. This

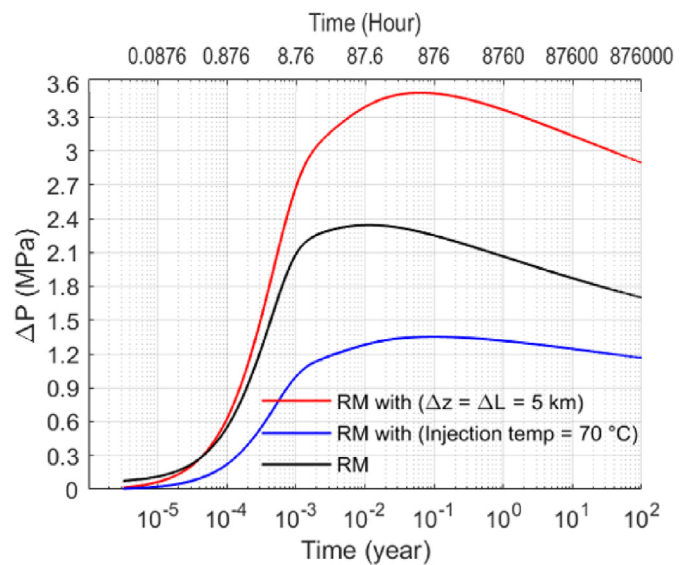


**Fig. 16.** Comparison between the effects of inlet temperature increment and system enlargement ( $\Delta z = \Delta l = 5 \text{ km}$ ) on the extraction pressure of the reference model (RM stands for reference model). System enlargement is superior to the injection temperature increment to enhance thermosiphoning.

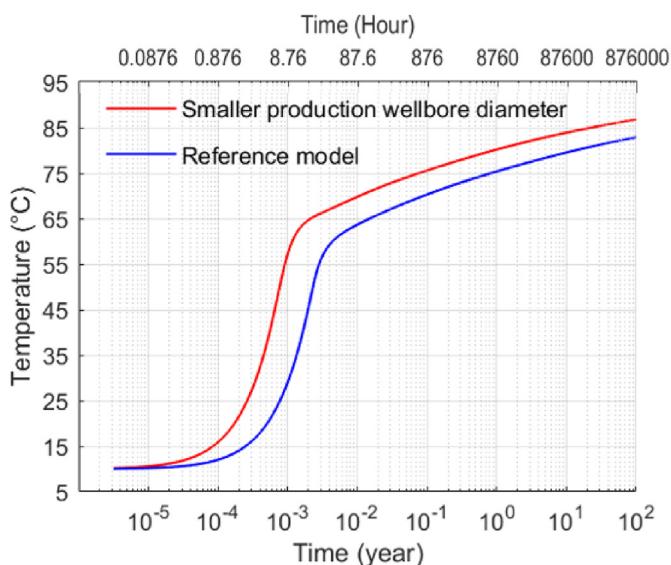


Fig. 17. Impact of decreasing production wellbore diameter on the production temperature over time. The smaller wellbore diameter leads to a higher extraction temperature over time.

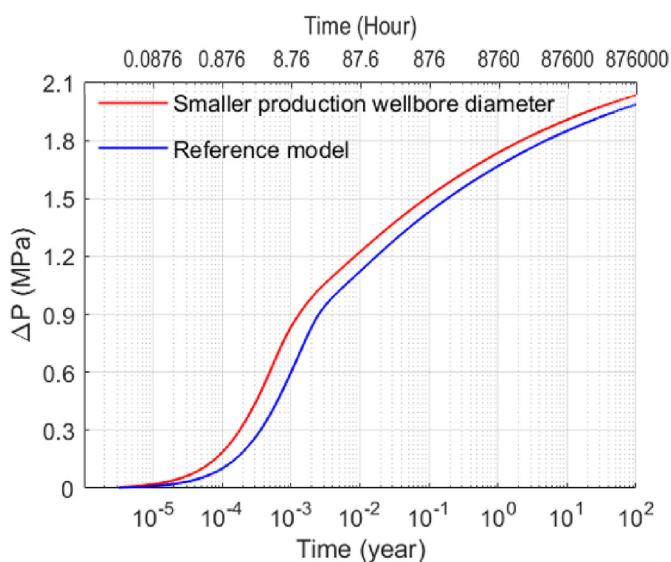


Fig. 18. Impact of decreasing production wellbore diameter on the production pressure over time. The smaller wellbore diameter leads to a higher pressure difference between injection and extraction points.

pressure gradient improvement is also beneficial for the case of the thermosiphon flow since a higher excess pressure is available at the outlet for the fluid circulation.

6. Conclusion

Our investigation indicates new insights to forecasting CDG behavior by state-of-the-art numerical simulations considering the coupling of mass, momentum, and energy conservation equations with an appropriate equation of state (EOS) and analytical lateral heat model. Novel approaches were proposed to make the CDG system a strong competitor to other conventional geothermal systems.

As addressed by Budiono et al. [42], drilling cost is the main

hurdle limiting the contribution of CDG systems to green energy generation. Our simulations allow to advance this knowledge and to identify beneficial factors for increasing the economic efficiency of CDG systems. One of these novel approaches was the evaluation of natural thermosiphon flow for fluid circulation that will significantly reduce the pumping energy. Also, the conditions for stability of thermosiphon flow under various pressure losses at surface facilities and geometrical configurations are demonstrated for the first time. The results are important as the two factors “high extraction temperature” and “stable thermosiphon flow rate” enable a cost-efficient power generation. Unique contributions are provided to the casing program and to the conceptual scheme to determine an optimum length of insulation.

Operation with CDG systems is associated with a rather stable production temperature over a span of a century. This effect was evaluated under various geometrical configurations (e.g., wellbore diameter) and operational parameters (e.g., flow rate). Also, thermosiphon flow generation can be considered atypical behavior of CDG systems. This flow could even be valve-controlled but has restrictions in geometry. Finally, various operational scenarios, as well as system configurations, are elaborately discussed to enhance the system’s longevity, to decrease pumping energy, to increase extracted power, and to diminish drilling costs.

The key findings of this study are summarized as:

1. In general, the CDG system presented in this study is capable of generating thermosiphon flow. Several case studies considering different parameters and configurations were evaluated. Even in the most extreme condition of the pressure loss in surface facilities (900 kPa), the triggered thermosiphon flow rate of the 12 km long reference case is higher than 11 L/s. Operating this flow can result in the production of approx. 2 MW thermal power at an average extraction temperature of 50 °C. Restricting this flow rate to 5 L/s increases the average extraction to approximately 80 °C. Thermosiphon flow rate is highly geometry sensitive. A shallower 3 km depth system (but identical total borehole length) results in 66% of the thermosiphon flow rate of the 4 km deep reference case. Reduced diameters results in a considerable lower thermosiphon flow rate. As such a reduction of 4” lowers the flow rate by 4 L/s due to higher friction losses.
2. A prolonged thermal exchange duration and a convenient convective heat transfer factor can avoid the huge temperature drop along all wellbores over time, and they also stabilize the extraction temperature. While operating with a flow rate of 10 L/s results in 12 °C extraction temperature drop over the project lifetime (67 °C after the first year, 55 °C after 100 years), the flow rate of 1 L/s yields 9 °C temperature increment over this period (75 °C after the first year, 84 °C after 100 years). Consequently, it was shown that not only the extraction temperature doesn’t reduce considerably over time, but also the generated power and production temperature continuously enhance over a project lifetime of one century. Therefore, an appropriate adjustment of CDG systems results in considerable enhancement of system’s longevity and preventing the initial extraction temperature drop, which is the major limitation in utilizing closed geothermal systems.
3. It is demonstrated that the reduction of the production well diameter enhances the extraction temperature through the increase of the circulating fluid velocity and the reduction of heat loss in this section of the CDG system. Subtracting 4” from the production wellbore diameter of the reference case increases the extraction temperature by 5 °C. It is also helpful for the generation of the thermosiphon flow, which is a function of temperature/density contrast between vertical wells. Consequently, the decrease of production wellbore diameter reduces

the relative drilling costs, improves power production, and diminishes the energy required for pumping the fluid.

- It is disclosed that the insulation length in the production well is absolutely dependent on geological settings. The increase of the thermal conductivity of the lower geological layer from 2 to  $4 \text{ W m}^{-1}\text{K}^{-1}$  raises the optimum insulation length from 2 km to 2.8 km. Nevertheless, insulation extension is independent of the subsurface temperature gradient, assuming the same geometrical configuration and operational parameters (i.e., flow rate, injection temperature, and pressure). For all the subsurface temperature gradients of 30, 35, and  $40 \text{ }^\circ\text{C}/\text{km}$ , the optimum insulation length is 2.5 km. Therefore, operating in regions with higher subsurface temperature increases the power production temperature and net generated power without the necessity of extending the insulation layer.

CDG systems certainly have a good perspective in urban areas. They should be considered as a long-term investment, providing energy to domestic heat systems or district heating grids over a period of more than 100 years. CDG systems could be enhanced by multi-lateral structures to scale up the generated power and decrease the ratio of extracted energy to the total length of the system. The herein presented analysis of thermal power production in vertical and horizontal wellbore sections will be further advanced for the design of multilateral CDG systems.

#### CRedit authorship contribution statement

**Morteza Esmailpour:** Investigation, Methodology, Validation, Writing – original draft, Visualization. **Maziar Gholami Korzani:** Methodology, Writing – review & editing, Supervision. **Thomas Kohl:** Writing – review & editing, Supervision, Project administration.

#### Declaration of competing interest

The authors declare that they have no known competing financial interests or personal relationships that could have appeared to influence the work reported in this paper.

#### Acknowledgment

The study is part of the subtopic “Geoenergy” in the program “MTET - Materials and Technologies for the Energy Transition” of the Helmholtz Association.

#### Nomenclature

$\rho$	Density ( $\text{Kg} \cdot \text{m}^{-3}$ )
$v$	Velocity ( $\text{m} \cdot \text{s}^{-1}$ )
$m$	Mass source term ( $\text{Kg} \cdot \text{m}^{-3} \cdot \text{s}^{-1}$ )
$P$	Pressure ( $\text{N} \cdot \text{m}^{-2}$ )
$g$	Gravity ( $\text{m} \cdot \text{s}^{-2}$ )
$f$	Friction factor
$d$	Hydraulic diameter (m)
$h$	Enthalpy ( $\text{J} \cdot \text{kg}^{-1}$ )
$q$	Lateral heat flow ( $\text{J} \cdot \text{m}^{-1} \cdot \text{s}^{-1}$ )
$Q$	Heat source/sink ( $\text{J} \cdot \text{m}^{-3} \cdot \text{s}^{-1}$ )
$r_{to}$	Outside radius of inner tubing (m)
$U_{to}$	Overall heat transfer coefficient
$T_f$	Fluid temperature ( $^\circ\text{C}$ )
$T_{cf}$	Temperature at fluid/cement interface ( $^\circ\text{C}$ )
TAEM	Total Absorbed Energy per Meter of system
RHS	Right Hand Side
PDE	Partial Differential Equation

TVD	Total Vertical Depth
MD	Measured Depth

#### References

- S. Eyerer, C. Schiffelechner, S. Hofbauer, et al., Combined heat and power from hydrothermal geothermal resources in Germany: an assessment of the potential, *Renew. Sustain. Energy Rev.* 120 (2020), 109661.
- M. Gholami Korzani, S. Held, T. Kohl, Numerical based filtering concept for feasibility evaluation and reservoir performance enhancement of hydrothermal doublet systems, *J. Petrol. Sci. Eng.* 190 (2020), 106803.
- A. Santilano, E. Trumpy, G. Gola, et al., A methodology for assessing the favourability of geopressured-geothermal systems in sedimentary basin plays: a case study in abruzzo (Italy), *Geofluids* 2019 (2019) 1–28.
- R. Egert, M. Gholami Korzani, S. Held, et al., Implications on large-scale flow of the fractured EGS reservoir Soultz inferred from hydraulic data and tracer experiments, *Geothermics* 84 (2020), 101749.
- S. Li, Y. Wang, K. Zhang, Exergy analysis of heat extraction from hot dry rock by enclosed Water recycling in a horizontal Well, *Geothermics* 86 (2020), 101867.
- A. Jentsch, E. Jolie, D.G. Jones, et al., Magmatic volatiles to assess permeable volcano-tectonic structures in the Los Humeros geothermal field, Mexico, *J. Volcanol. Geoth. Res.* 394 (2020), 106820.
- J. Nouraliee, D. Ebrahimi, A. Dashti, et al., Appraising Mahallat Geothermal Region using thermal surveying data accompanied by the geological, geochemical and gravity analyses, *Sci. Rep.* 11 (1) (2021), 12190.
- R. Egert, F. Nitschke, M. Gholami Korzani, et al., Stochastic 3D Navier-Stokes flow in self-affine fracture geometries controlled by anisotropy and channeling, *Geophys. Res. Lett.* 48 (9) (2021).
- G. Jharap, L.P. van Leeuwen, R. Mout, et al., Ensuring safe growth of the geothermal energy sector in The Netherlands by proactively addressing risks and hazards, *Neth. J. Geosci.* 99 (2020).
- Q. Gan, Q. Lei, Induced fault reactivation by thermal perturbation in enhanced geothermal systems, *Geothermics* 86 (2020), 101814.
- K. Stricker, J.C. Grimmer, R. Egert, et al., The potential of depleted oil reservoirs for high-temperature storage systems, *Energies* 13 (24) (2020) 6510.
- Z. Ma, L. Xia, X. Gong, et al., Recent advances and development in optimal design and control of ground source heat pump systems, *Renew. Sustain. Energy Rev.* 131 (2020), 110001.
- D. Roy, T. Chakraborty, D. Basu, et al., Feasibility and performance of ground source heat pump systems for commercial applications in tropical and subtropical climates, *Renew. Energy* 152 (2020) 467–483.
- L. Rybach, T. Kohl, The geothermal heat pump boom in Switzerland and its background, in: *Proceedings of International Geothermal Congress, Reykjavik, Iceland, 2003*.
- X. Song, Y. Shi, G. Li, et al., Heat extraction performance simulation for various configurations of a downhole heat exchanger geothermal system, *Energy* 141 (2017) 1489–1503.
- S. Signorelli, T. Kohl, L. Rybach, Sustainability of production from borehole heat exchanger fields, in: *Proceedings of World Geothermal Congress, Antalya, Turkey, 2005*.
- Y. Shi, X. Song, G. Li, et al., Numerical investigation on heat extraction performance of a downhole heat exchanger geothermal system, *Appl. Therm. Eng.* 134 (2018) 513–526.
- G. Wang, X. Song, Y. Shi, et al., Heat extraction analysis of a novel multilateral-well coaxial closed-loop geothermal system, *Renew. Energy* 163 (2021) 974–986.
- C.S. Blázquez, A.F. Martín, I.M. Nieto, et al., Analysis and study of different grouting materials in vertical geothermal closed-loop systems, *Renew. Energy* 114 (2017) 1189–1200.
- A. Eswiasi, P. Mukhopadhyaya, Critical review on efficiency of ground heat exchangers in heat pump systems, *Clean Technol.* 2 (2) (2020) 204–224.
- S. Kumar, K. Murugesan, Optimization of geothermal interaction of a double U-tube borehole heat exchanger for space heating and cooling applications using Taguchi method and utility concept, *Geothermics* 83 (2020), 101723.
- B. Sanner, Summary of EGC 2019 country update reports on geothermal energy in Europe, in: *Proceedings of European Geothermal Congress, Den Haag, Netherlands, 2019*.
- M. Kaltschmitt, E. Huenges, H. Wolff, et al., *Energy from Geothermal Energy*, Springer spectrum, 1999.
- M. Kharseh, M. Al-Khawaja, F. Hassani, Optimal utilization of geothermal heat from abandoned oil wells for power generation, *Appl. Therm. Eng.* 153 (2019) 536–542.
- Y.-L. Nian, W.-L. Cheng, Evaluation of geothermal heating from abandoned oil wells, *Energy* 142 (2018) 592–607.
- R.A. Caulk, I. Tomac, Reuse of abandoned oil and gas wells for geothermal energy production, *Renew. Energy* 112 (2017) 388–397.
- T. Kohl, R. Brenni, W. Eugster, System performance of a deep borehole heat exchanger, *Geothermics* 31 (6) (2002) 687–708.
- T. Kohl, M. Salton, L. Rybach, Data analysis of the deep borehole heat exchanger plant Weissbad (Switzerland), in: *Proceedings of World Geothermal Congress, Kyushu-Tohoku, Japan, 2000*.
- Y. Huang, Y. Zhang, Y. Xie, et al., Long-term thermal performance analysis of

- deep coaxial borehole heat exchanger based on field test, *J. Clean. Prod.* 278 (2021), 123396.
- [30] E.D. Kerme, A.S. Fung, Comprehensive simulation based thermal performance comparison between single and double U-tube borehole heat exchanger and sensitivity analysis, *Energy Build.* 241 (2021), 110876.
- [31] E.M. Salilih, N.H. Abu-Hamdeh, H.F. Oztop, Analysis of double U-tube ground heat exchanger for renewable energy applications with two-region simulation model by combining analytical and numerical techniques, *Int. Commun. Heat Mass Tran.* 123 (2021), 105144.
- [32] N. Jamshidi, A. Mosaffa, Investigating the effects of geometric parameters on finned conical helical geothermal heat exchanger and its energy extraction capability, *Geothermics* 76 (2018) 177–189.
- [33] J.D. Templeton, S.A. Ghoreishi-Madiseh, F.P. Hassani, et al., Numerical and experimental study of transient conjugate heat transfer in helical closed-loop geothermal heat exchangers for application of thermal energy storage in backfilled mine stopes, *Int. J. Energy Res.* 44 (12) (2020) 9609–9616.
- [34] H. Javadi, S.S. Mousavi Ajarostaghi, M. Pourfallah, et al., Performance analysis of helical ground heat exchangers with different configurations, *Appl. Therm. Eng.* 154 (2019) 24–36.
- [35] H. Javadi, S.S. Mousavi Ajarostaghi, M.A. Rosen, et al., Performance of ground heat exchangers: a comprehensive review of recent advances, *Energy* 178 (2019) 207–233.
- [36] E. Rossi, S. Jamali, M.O. Saar, et al., Field test of a combined thermo-mechanical drilling technology. Mode I: thermal spallation drilling, *J. Petrol. Sci. Eng.* 190 (2020), 107005.
- [37] E. Rossi, S. Jamali, D. Schwarz, et al., Field test of a combined thermo-mechanical drilling technology. Mode II: flame-assisted rotary drilling, *J. Petrol. Sci. Eng.* 190 (2020), 106880.
- [38] E. Rossi, S. Jamali, V. Wittig, et al., A combined thermo-mechanical drilling technology for deep geothermal and hard rock reservoirs, *Geothermics* 85 (2020), 101771.
- [39] S. Elkhatny, H. Gamal, A. Ahmed, et al., A novel solution for severe loss prevention while drilling deep wells, *Sustainability* 12 (4) (2020) 1339.
- [40] J. Wang, F. Nitschke, M. Gholami Korzani, et al., Temperature log simulations in high-enthalpy boreholes, *Geoth. Energy* 7 (1) (2019).
- [41] 9/16, Eavor – the First Truly Scalable Form of Clean Baseload Power, 2021, <https://www.eavor.com/>.
- [42] A. Budiono, S. Suyitno, I. Rosyadi, et al., A systematic review of the design and heat transfer performance of enhanced closed-loop geothermal systems, *Energies* 15 (3) (2022) 742.
- [43] X. Song, Y. Shi, G. Li, et al., Numerical analysis of the heat production performance of a closed loop geothermal system, *Renew. Energy* 120 (2018) 365–378.
- [44] F. Sun, Y. Yao, G. Li, et al., Geothermal energy development by circulating CO<sub>2</sub> in a U-shaped closed loop geothermal system, *Energy Convers. Manag.* 174 (2018) 971–982.
- [45] X. Sun, Z. Wang, Y. Liao, et al., Geothermal energy production utilizing a U-shaped well in combination with supercritical CO<sub>2</sub> circulation, *Appl. Therm. Eng.* 151 (2019) 523–535.
- [46] W. Yuan, Z. Chen, S.E. Grasby, et al., Closed-loop geothermal energy recovery from deep high enthalpy systems, *Renew. Energy* 177 (2021) 976–991.
- [47] A. Ghavidel, R. Gracie, M.B. Dusseault, Transient heat transfer in a horizontal well in hot dry rock – model, solution, and response surfaces for practical inputs, *Appl. Therm. Eng.* 195 (2021), 117158.
- [48] A. Fallah, Q. Gu, D. Chen, et al., Globally scalable geothermal energy production through managed pressure operation control of deep closed-loop well systems, *Energy Convers. Manag.* 236 (2021), 114056.
- [49] W. Zhang, W. Li, B.R. Sørensen, et al., Comparative analysis of heat transfer performance of coaxial pipe and U-type deep borehole heat exchangers, *Geothermics* 96 (2021), 102220.
- [50] J. Chen, S. Feng, Evaluating a large geothermal absorber's energy extraction and storage performance in a common geological condition, *Appl. Energy* 279 (2020), 115793.
- [51] M. Esmailpour, M. Gholami Korzani, Enhancement of immiscible two-phase displacement flow by introducing nanoparticles and employing electro- and magneto-hydrodynamics, *J. Petrol. Sci. Eng.* 196 (2021), 108044.
- [52] M. Esmailpour, M. Gholami Korzani, Analyzing impacts of interfacial instabilities on the sweeping power of Newtonian fluids to immiscibly displace power-law materials, *Processes* 9 (5) (2021) 742.
- [53] M. Esmailpour, M. Gholami Korzani, T. Kohl, Performance Analyses of Deep Closed-Loop U-Shaped Heat Exchanger System with a Long Horizontal Extension: 46th Workshop on Geothermal Reservoir Engineering, Stanford University, Stanford, California, 2021.
- [54] M. Gholami Korzani, F. Nitschke, S. Held, et al., The Development of a Fully Coupled Wellbore-Reservoir Simulator for Geothermal Application, vol. 43, 2019.
- [55] D. Gaston, C. Newman, G. Hansen, et al., MOOSE: a parallel computational framework for coupled systems of nonlinear equations, *Nucl. Eng. Des.* 239 (10) (2009) 1768–1778.
- [56] C.J. Permann, D.R. Gaston, D. Andrš, et al., MOOSE: enabling massively parallel multiphysics simulation, *Software* 11 (2020), 100430.
- [57] S. Livescu, L.J. Durlafsky, K. Aziz, et al., A fully-coupled thermal multiphase wellbore flow model for use in reservoir simulation, *J. Petrol. Sci. Eng.* 71 (3–4) (2010) 138–146.
- [58] M.L. Huber, R.A. Perkins, A. Laesecke, et al., New international formulation for the viscosity of H<sub>2</sub>O, *J. Phys. Chem. Ref. Data* 38 (2) (2009) 101–125.
- [59] S. Phillips, A. Igbene, J. Fair, et al., A Technical Databook for Geothermal Energy Utilization, Lawrence Berkeley National Laboratory, 1981.
- [60] G.P. Willhite, Over-all heat transfer coefficients in steam and hot water injection wells, *J. Petrol. Technol.* 19 (5) (1967) 607–615.
- [61] I.E. Idelchik, *Handbook of Hydraulic Resistance*, 1996. New York.
- [62] H. Tang, B. Xu, A.R. Hasan, et al., Modeling wellbore heat exchangers: fully numerical to fully analytical solutions, *Renew. Energy* 133 (2019) 1124–1135.